

Ag Modified SnS₂ Monolayer as a Potential Sensing Material for C₄F₇N Decompositions: A Density Functional Theory Study

Xiangyu Tan, Zhimin Na, Ran Zhuo, Fangrong Zhou, Dibo Wang, Longchang Zhu, and Peng Wu*



Cite This: *ACS Omega* 2024, 9, 23523–23530



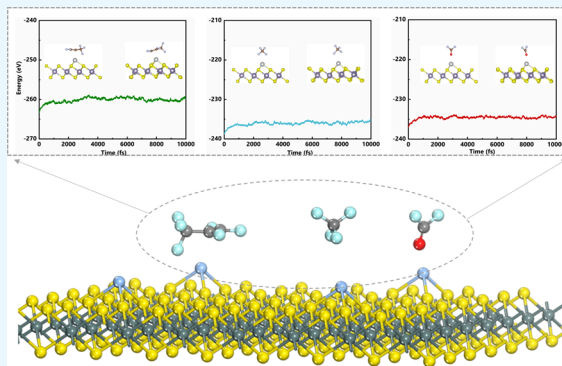
Read Online

ACCESS |

Metrics & More

Article Recommendations

ABSTRACT: As the field of 2D materials rapidly evolves, substances such as graphene, metal dichalcogenides, MXenes, and MBenes have garnered extensive attention from scholars in the gas sensing domain due to their unique and superior properties. Based on first-principles calculations, this work explored the adsorption characteristics of both intrinsic and silver (Ag) doped tin disulfide (SnS₂) toward the decomposition components of the insulating medium C₄F₇N (namely, CF₄, C₃F₆, and COF₂), encompassing the adsorption energy, charge transfer, density of state (DOS), band structure, and adsorption stability. The results indicated that Ag-doped SnS₂ exhibited an effective and stable adsorption for C₃F₆ and COF₂, whereas its adsorption for CF₄ was comparatively weaker. Additionally, the potential for Ag-SnS₂ in detecting C₃F₆ was highlighted, inferred from the contributions of the band gap variations. This research provides theoretical guidance for the application of Ag-SnS₂ as a sensing material in assessing the operational status of gas-insulated equipment.



INTRODUCTION

Sulfur hexafluoride (SF₆) is renowned for its exceptional electrical insulating properties and is widely utilized in the power industry's high-voltage equipment as either an insulator or an arc-quenching medium. However, its considerable Global Warming Potential (GWP) of 23,900 has led to its inclusion in international environmental treaties, such as the Kyoto Protocol and the Paris Agreement, resulting in its classification as a restricted-use greenhouse gas.^{1–3} To mitigate reliance on SF₆ and its environmental impact, the power industry has proposed the eco-friendly insulating gas perfluoroisobutyronitrile (C₄F₇N) as an alternative for use in gas-insulated equipment (GIE). C₄F₇N offers an insulation capacity of 2.2 times that of SF₆ but with a GWP that is only 1/11th of SF₆'s, an ozone depletion potential of zero, and an atmospheric lifetime of 22 years.^{4–7} Because of its high liquefaction temperature of −4.7 °C, C₄F₇N is typically blended with lower liquefaction temperature gases such as CO₂ and N₂, to maintain functional reliability under low-temperature conditions.^{3,8–11} Moreover, for the GIE, internal defects such as free metallic particles, metal protrusions, and poor conductor contact are inevitable during transportation, assembly, and operation. Over time, these defects may induce internal faults like partial discharges and partial overheating.¹² The insulation medium will undergo a certain degree of decomposition and yield various fault-induced decomposition products, undermining the internal insulation stability of GIE and elevating the risk of critical malfunctions and potential power outages.¹³ In

the case of C₄F₇N based GIE, partial discharges CAN result in the generation of gases such as C₃F₆, C₂F₆, C₃F₈, CF₄, and CO. Notably, the concentration of CF₄ demonstrates a strong linear correlation with both the intensity and duration of the discharge.¹⁴ In scenarios of partial overheating, the primary decomposition products of the C₄F₇N mixed gas include C₃F₆, CO, CF₄, C₂F₆, CF₃CN, COF₂, and C₂N₂. Specially, under the catalytic influence of common internal materials like copper, EPDM rubber, and aluminum, C₃F₆ can form at temperatures significantly lower than the normal decomposition temperature of C₄F₇N, providing a valuable indicator for the early detection of overheating faults.^{1,15} Furthermore, the concentration of COF₂ establishes a reliable linear relationship with overheating temperatures above 400 °C, serving as a useful metric for assessing the severity of such faults.¹⁶ The qualitative and quantitative analysis of these signature gases paves the way for the early detection and remediation of incipient faults within the GIE. This proactive approach prevents the progression of these faults into more serious complications, thereby

Received: January 21, 2024

Revised: April 26, 2024

Accepted: May 9, 2024

Published: May 22, 2024



safeguarding the continuous and stable operation of electrical power systems.

Nanomaterial-based resistive gas sensing technology is a highly efficient method for acquiring gas fingerprint information in spaces, characterized by its high sensitivity, rapid response, portability, and high integration. This technology finds widespread application across various fields.^{17,18} In the quest for high-performance sensing materials, scholars in related fields have identified the significant potential of two-dimensional nanomaterials, offering diverse solutions for achieving low detection limits, broad detection ranges, and specific responses in gas sensing. Among these materials, SnS₂, known for its large specific surface area, high carrier mobility, tunable band gap, as well as its chemical stability in oxygen and thermal atmosphere, has garnered considerable attention in the gas sensing domain and demonstrated outstanding performance.^{19–22} For example, the hollow structure of SnS₂ synthesized by Liu and colleagues demonstrates high sensitivity for detecting NO₂ at room temperature (25 °C) under ultraviolet irradiation.²³ Eom et al. enhanced the room-temperature response of SnS₂ nanoflowers to NO₂ using visible light, achieving exceptionally high sensing selectivity and a low detection limit.²⁴ Similarly, intrinsic SnS₂ has been widely applied in the detection of other toxic industrial gases, such as NH₃, aldehydes, and ketones.^{25–27} However, the inherent high sensitivity of SnS₂ in gas detection is commonly counterbalanced by its slow response and recovery times, which significantly curtail its practical use. Recent research has demonstrated that the introduction of a noble metal or constructing heterostructures can effectively transform the electronic structure of SnS₂. These modifications not only elevate carrier mobility but also enhance interfacial charge transfer, resulting in a marked improvement in both the sensitivity and the response-recovery dynamics of pristine SnS₂ for targeted gas detection. The Au doped SnS₂ proposed by Zhu et al. was used to fabricate NO₂ gas sensors. It was found that because of the spillover effect of Au atom, the response and recovery times of the gas sensors were accelerated from 393.6 and 451.2 s to 127.6 and 255.2 s.²⁸ Recently, Ag were proven to be effective in improving the sensing performance of SnS₂ with certain repeatability and stability.^{29–31} To further meet the demands for high sensitivity and rapid response in engineering gas sensing applications, this study will investigate the adsorption characteristics of Ag doped SnS₂ toward decomposition by product of C₄F₇N, including CF₄, C₃F₆, and COF₂.

In this work, a Ag-doped SnS₂ monolayer was proposed for the first time as a sensing material to explore its adsorption and sensing characteristics for CF₄, C₃F₆, and COF₂ using density functional theory (DFT) calculations. The adsorption performance and mechanisms for these three gas molecules on Ag-SnS₂ were revealed by analyzing the structural parameters, adsorption energy, charge transfer, DOS, band structure, adsorption stability, and recovery time of each adsorption system. The findings not only provide insights for online fault monitoring and diagnosis in novel power systems but also expand the application scope of SnS₂ materials.

THEORETICAL METHODS

The calculations in this work were carried out by first-principles calculations on the basis of DFT using the Vienna Ab initio Simulation Package (VASP). For the electron–ion interaction, the projected augmented wave (PAW) method

with ultrasoft pseudopotentials was employed for description,^{32,33} and the electron exchange–correlation interaction was represented using the Perdew–Burke–Ernzerhof (PBE) formula within the framework of the generalized gradient approximation (GGA).³⁴ The semiempirical dispersion correction method, Grimme’s DFT-D2, was utilized to correct interactions arising from weak van der Waals (vdWs) forces.³⁵ The initial SnS₂ supercell was constructed by a 4 × 4 × 1 structural expansion of the unit cell. For the geometric optimization and electronic structure calculations, the k-points were set to 4 × 4 × 1 in the Monkhorst–Pack grid. In the energy optimization of the system, the cutoff energy and the self-consistent field convergence threshold were set to 520 and 10^{−5} eV, respectively. The Gaussian smearing of 0.1 eV was utilized to calculate the electronic structure.³⁶ Interatomic forces were treated using the block Davidson iterative method, with the convergence criterion also based on force values; specifically, optimization was terminated when the force on an individual atom fell below 0.02 eV/Å. To prevent interlayer interactions from affecting the adsorption of gas molecules, a 20 Å vacuum layer was added between adjacent layers of SnS₂. Bader charge analysis was employed to compute the charge exchange behavior between intrinsic and Ag-doped SnS₂ substrates with CF₄, C₃F₆, and COF₂ gas molecules.³⁷ The cohesion energy (E_{co})³⁸ of Ag atom doping and the adsorption energy (E_{ads})³⁹ between gas molecules and the sensing substrate were calculated using the following formulas:

$$E_{\text{co}} = E_{\text{Ag/SnS}_2} - E_{\text{Ag}} - E_{\text{SnS}_2} \quad (1)$$

$$E_{\text{ads}} = E_{\text{gas/substrate}} - E_{\text{gas}} - E_{\text{substrate}} \quad (2)$$

where $E_{\text{Ag/SnS}_2}$ represents the energy of the Ag doped SnS₂ systems, E_{Ag} represents the energy of an Ag atom, and E_{SnS_2} represents the energy of the SnS₂ monolayer. $E_{\text{gas/substrate}}$, E_{gas} , and $E_{\text{substrate}}$ are the energies of the sensing substrate with gas molecules adsorbed, gas molecules, and sensing substrates, respectively. The charge exchanges between the gas molecule and sensing substrate were denoted as Q_{t} . A positive Q_{t} value indicates electron loss from the gas molecule, whereas a negative value signifies electron gain from the sensing structure.

RESULT AND DISCUSSION

Geometric Structure and Parameters. Figure 1 presents the most energy favorable structures of intrinsic SnS₂ and gas molecules C₃F₆, COF₂, and CF₄ after geometry optimization. In Figure 1a, SnS₂ is illustrated in a S–Sn–S sandwich conformation, where the Sn–S bond length measures 2.590 Å, aligning with values documented in the literature.^{40,41} Because of its surface symmetry, preferred adsorption sites for the gas molecules were identified at the centers of the red dashed boxes, as indicated in Figure 1a. As Figure 1b reveals, the symmetrical properties of COF₂ and CF₄ display significant symmetrical properties. The initial adsorption orientations for COF₂ were established with the molecule parallel to the SnS₂ plane and either an O atom or two F atoms oriented perpendicularly downward. For CF₄, the proposed approaches toward the SnS₂ sensing surface involved configurations with one, two, or three C–F bonds oriented downward. The asymmetric structure of C₃F₆, however, complicates the consideration of all possible adsorption scenarios. Consequently, this study selected initial adsorption orientations, both perpendicular and parallel to SnS₂, based on the plane

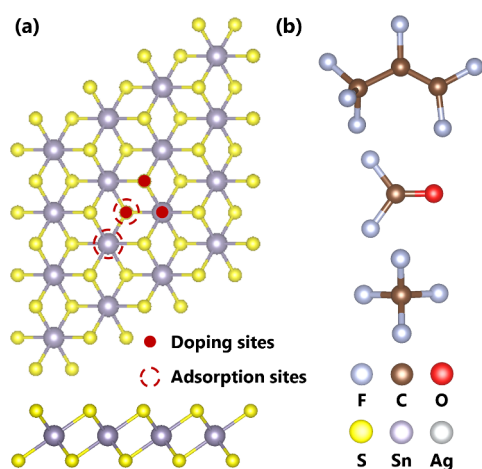


Figure 1. Optimized structures of (a) SnS₂, (b) C₃F₆, COF₂, and CF₄.

constituted by the central C=C functional group of the molecule. Upon the most stable Ag-SnS₂ structure, three potential Ag atom doping sites were taken into account: (a) atop the S atom (T_S), (b) atop the Sn atom (T_{Sn}), and (c) at the bridging site between the S and Sn atoms (B_{Sn-S}). Figure 2 displays the optimized structures for these doping sites, with their respective E_{co} being -1.929 , -1.717 , and -1.785 eV. Notably, model A, featuring Ag doping atop the S atom, showcased the highest E_{form} , suggesting that this site yields the most stable configuration on the SnS₂ surface. Accordingly, the adsorption of gas molecules on Ag-SnS₂ will be based on model A, with the adsorption site located atop the Ag atom and the orientation similar to that considered in the intrinsic SnS₂ system.

Based on the Ag-SnS₂ structure derived from model A, Figure 3 further presents the DOS and band structure of the system to investigate the impact of Ag atom doping on the electronic structure of SnS₂. As can be discerned from Figure 3a, the doping of Ag atoms caused a shift of the TDOS toward a lower energy level by approximately 9.000×10^{-1} eV and increased new energy states at several points. These results indicated that the doping of Ag atoms introduced impurity levels into the SnS₂ system, which align closely with the positions of the 4d atomic orbitals of Ag atoms depicted in Figure 3b. Moreover, the extensive overlap between the 4d

atomic orbitals of Ag and the 3p atomic orbitals of S atoms in the -2.021 to -5.673 eV range confirmed the high stability of the Ag-doped SnS₂ system. Figure 3c illustrates the band structure of SnS₂, with a corresponding band gap of 1.580 eV, consistent with existing research.⁴² Upon the addition of Ag atoms, both the conduction band minimum (CBM) and valence band maximum (VBM) of the system underwent a downward shift, and the band gap was reduced to 1.263 eV. This indicated that doping SnS₂ with Ag atoms is likely to enhance its electrical conductivity to a certain extent.

Adsorption Behavior of the C₃F₆ Molecule. After structural optimization and calculations of E_{ads} , the most stable adsorption configurations of C₃F₆ gas molecules on SnS₂ and Ag-SnS₂ surfaces are depicted in Figure 4a,b. It was observed that the C₃F₆ molecule approaches and adheres to the sensing substrate surfaces in a parallel orientation, achieving the most stable adsorption. The corresponding E_{ads} and Q_{t} values for these two systems were -1.976×10^{-1} and -2.299×10^{-1} eV and -6.512×10^{-2} and -5.070×10^{-2} e, respectively. In the SnS₂ adsorption system, the shortest atomic distance at the gas–solid interface is 3.002 Å between the S and F atoms, and no significant structural changes were observed in either the gas molecule or the substrate. In the Ag-SnS₂ system, a stronger interaction reduces the minimum distance between the C₃F₆ gas molecule and the sensing plane to 2.622 Å (C–Ag). Concurrently, the C–F bond length increased from 1.369 to 1.371 Å, indicating a strong interaction exerted by Ag atoms on specific atoms within the C₃F₆ molecule, primarily deriving from orbital hybridization between the atoms. As shown in Figure 4c, in the intrinsic SnS₂/C₃F₆ adsorption system, the degree of hybridization between the closest F atom 2p orbitals and the S atom 3p orbitals is relatively low, occurring only at energy levels of -3.271 , -3.645 , and -4.122 eV. This leads to a weaker overall interaction and lower E_{ads} between the molecule and the sensing substrate. However, in the Ag-SnS₂ adsorption system, there is more extensive overlap between the 4d orbitals of Ag atoms and the 2p orbitals of C and F atoms in the C₃F₆ at energy levels such as -7.991 , -7.383 , -6.516 , -5.642 , -4.541 , -3.060 eV, etc., resulting in stronger adsorption of C₃F₆ on the Ag-SnS₂ surface.

Adsorption Behavior of the CF₄ Molecule. Figure 5a,b presents the energetically optimal structures of CF₄ adsorbed on SnS₂ and Ag-SnS₂ surfaces, where CF₄ molecules

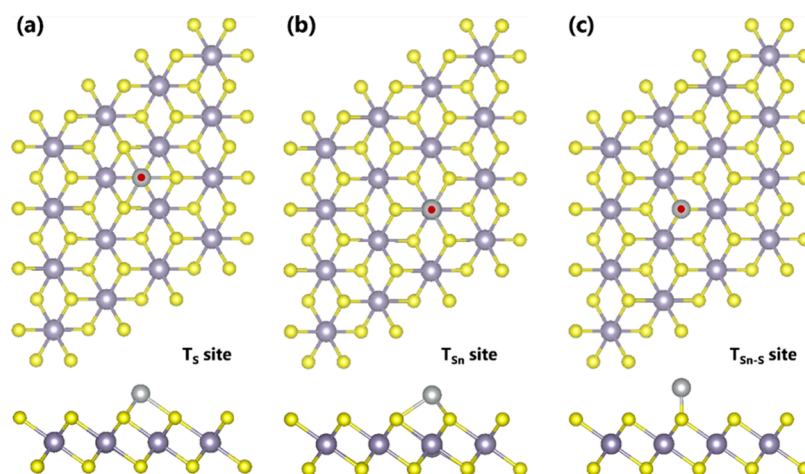


Figure 2. Optimized structures of Ag doped SnS₂ systems: (a) T_S site, (b) T_{Sn} site, and (c) B_{Sn-S} site.

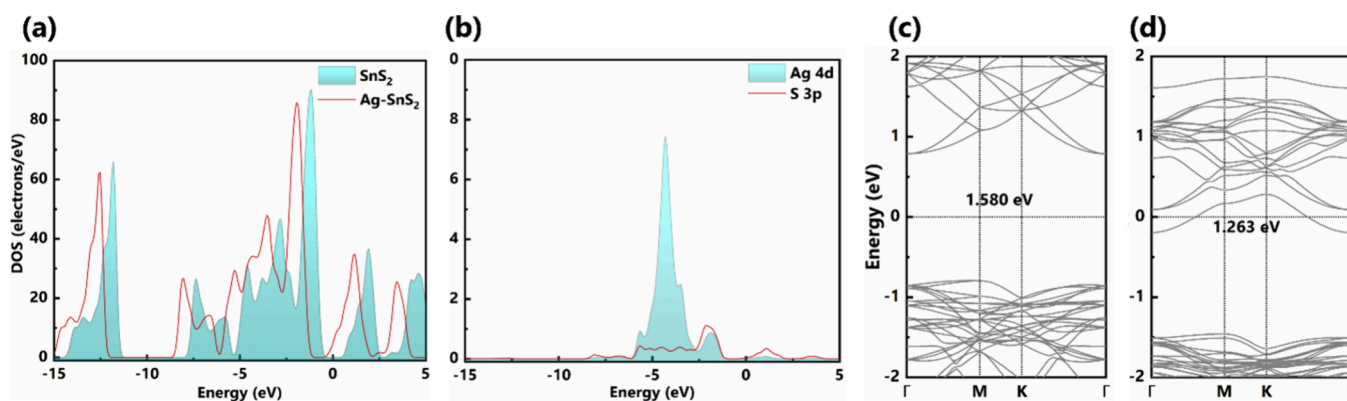


Figure 3. (a) TDOS of the pristine and Ag doped SnS₂ system, (b) PDOS of Ag and S atoms, and band structures of (c) pristine SnS₂ and (d) Ag doped SnS₂.

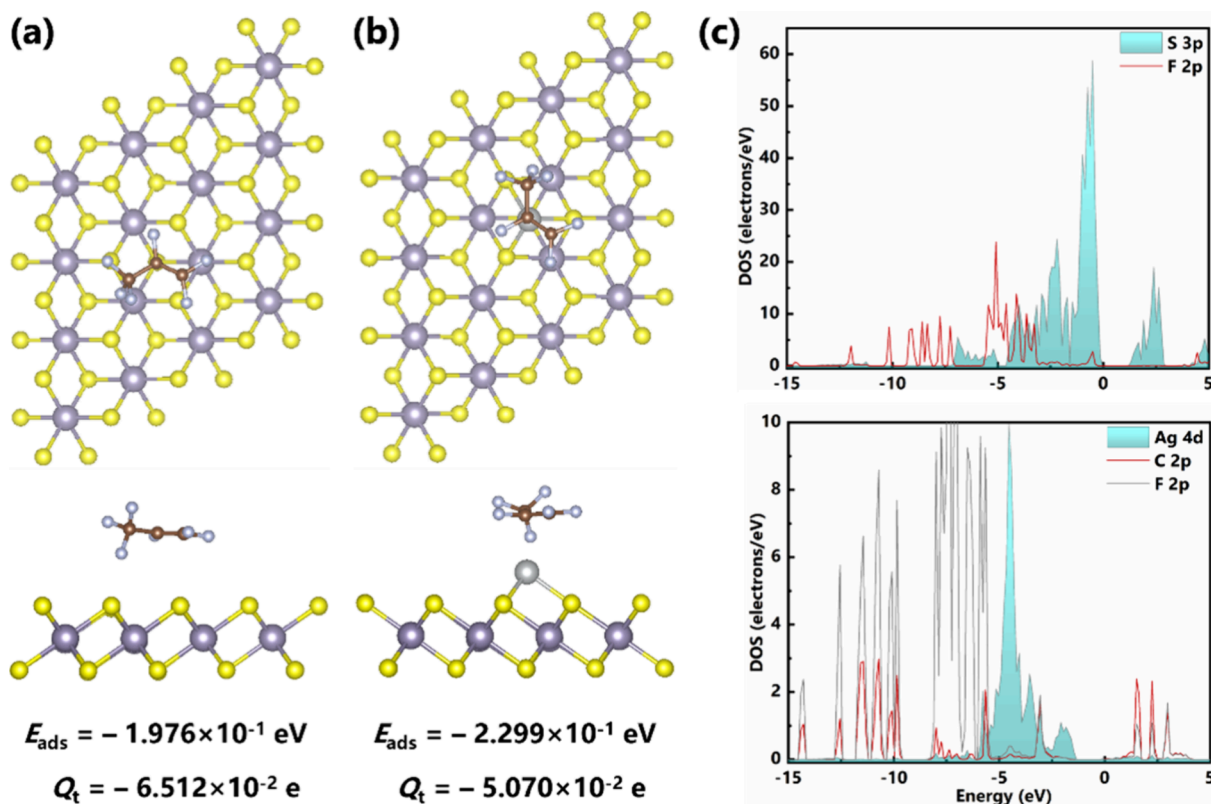


Figure 4. Optimized structures of C₃F₆ on (a) pristine SnS₂ and (b) Ag-SnS₂ and (c) PDOS of the C₃F₆ adsorbed pristine SnS₂ and Ag-SnS₂ systems.

approached the sensing surface with a single F atom and two F atoms, respectively. Owing to the highly symmetric geometry and electronic structure of CF₄, it is challenging for the gas molecule to undergo significant geometric deformation or charge exchange. Additionally, the inherent lack of active sites on the pristine SnS₂ surface hindered the adsorption of gas molecules, resulting in a relatively weak interaction in the SnS₂/CF₄ adsorption system, with E_{ads} and Q_t values of only -9.131×10^{-2} eV and -2.150×10^{-2} e, respectively. Meanwhile, the introduction of Ag atoms enhanced the reactivity of the SnS₂ surface, increasing the adsorption strength for CF₄. The minimum distance between them was reduced from 3.146 Å in the pristine SnS₂ system to 2.820 Å in the Ag-doped system, and the E_{ads} increased to -1.277×10^{-1} eV. Concurrently, the C–F bond length in CF₄ elongated from

1.345 to 1.358 Å but with a charge transfer of only $+3.700 \times 10^{-3}$ e. The PDOS presented in Figure 5c suggests an inverse correlation between the degree of atomic orbital hybridization and the adsorption strength before and after doping. Prior to doping with Ag atom, there was noticeable overlap between the 3p orbitals of S and the 2p orbitals of F at -5.611 , -5.110 , and -3.935 eV. Postdoping, the 2p orbitals of F and the 4d orbitals of Ag were positioned to the left and right of the 5.801 eV energy level, respectively, exhibiting almost no overlap. This phenomenon reveals the reason for the smaller Q_t in the CF₄/Ag-SnS₂ system compared to the CF₄/SnS₂ system, and the interactions between the CF₄ gas molecule and the sensing substrates were characterized by weak physical adsorptions.

Adsorption Behavior of the COF₂ Molecule. Figure 6a,b illustrates that on SnS₂ and Ag-SnS₂ surfaces, COF₂

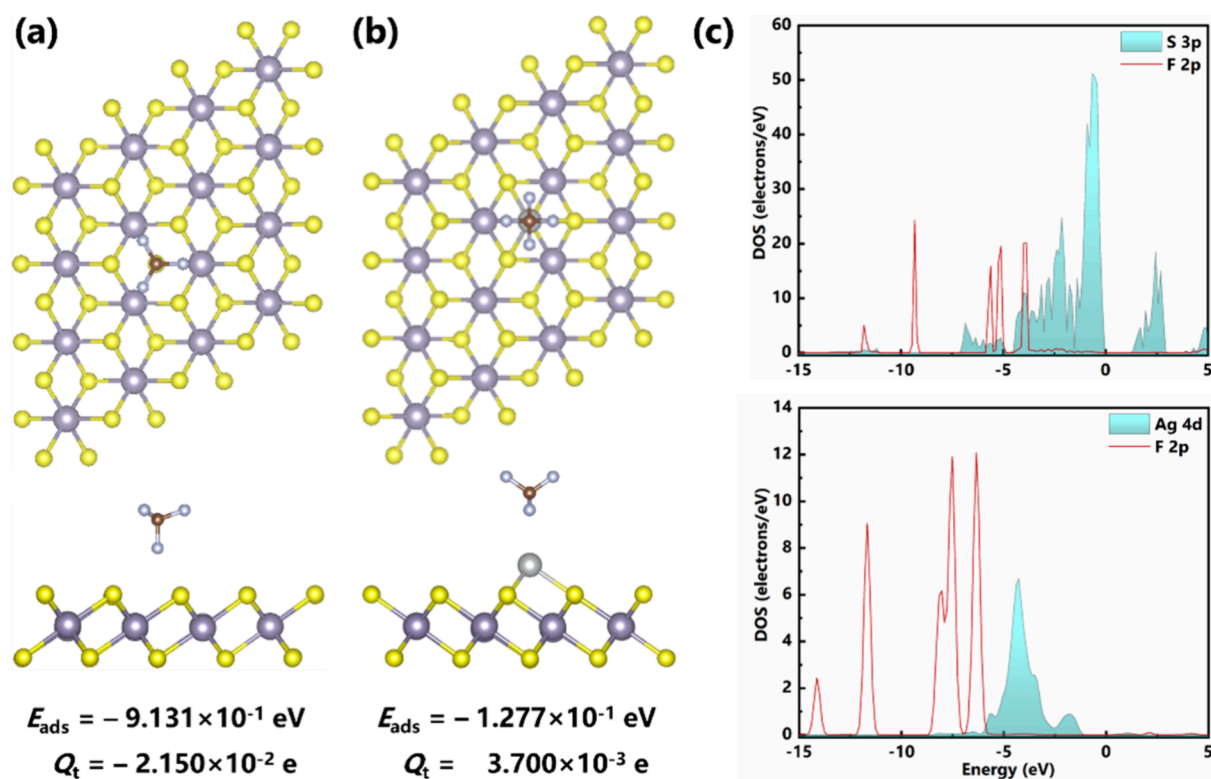


Figure 5. Optimized structures of CF_4 on (a) pristine SnS_2 and (b) Ag-SnS_2 and (c) PDOS of the CF_4 adsorbed pristine SnS_2 and Ag-SnS_2 systems.

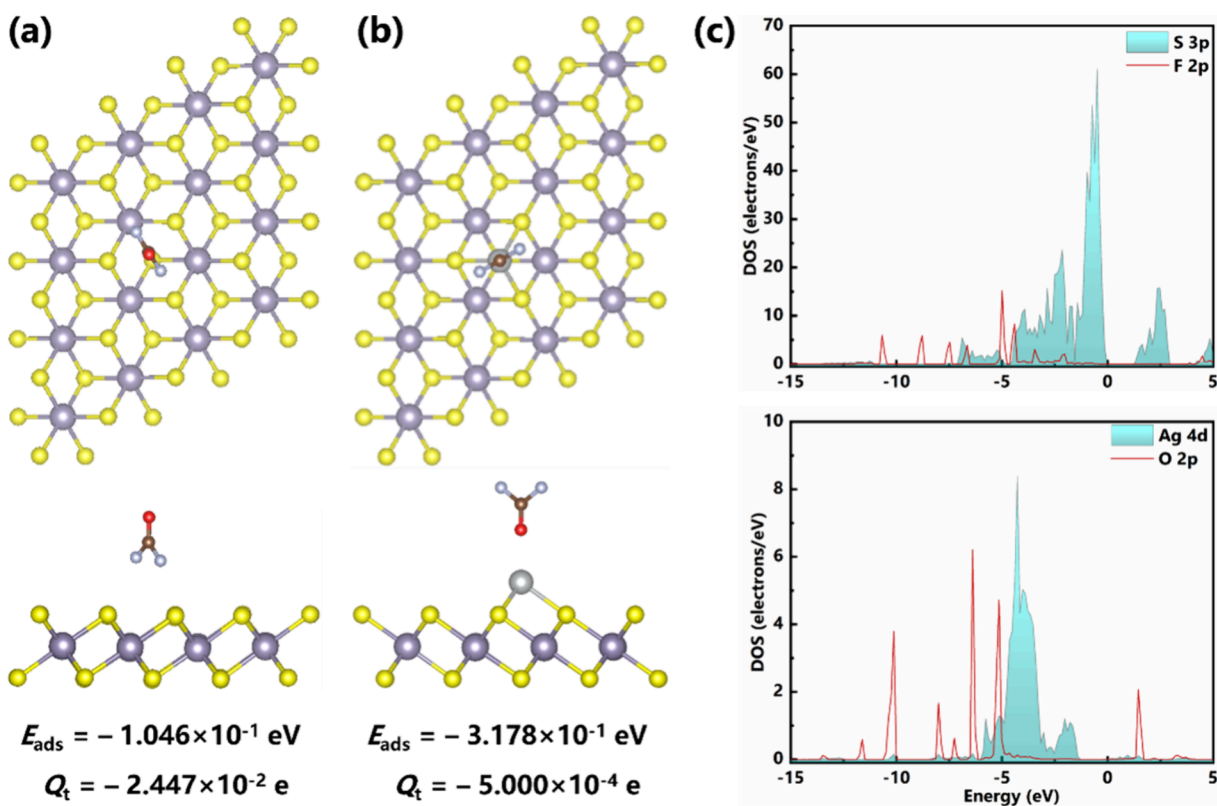


Figure 6. Optimized structures of COF_2 on (a) pristine SnS_2 and (b) Ag-SnS_2 and (c) PDOS of the COF_2 adsorbed pristine SnS_2 and Ag-SnS_2 systems.

molecules predominantly adsorbed via F and O atoms, respectively. The COF_2 - SnS_2 interaction was characterized by a minimal atomic separation of 3.08 Å accompanied by an

E_{ads} of $-1.046 \times 10^{-1} \text{ eV}$ and a Q_t of $-2.447 \times 10^{-2} \text{ e}$. This adsorption strength lay between those observed for CF_4 and C_3F_6 , without notable alterations in molecular conformation.

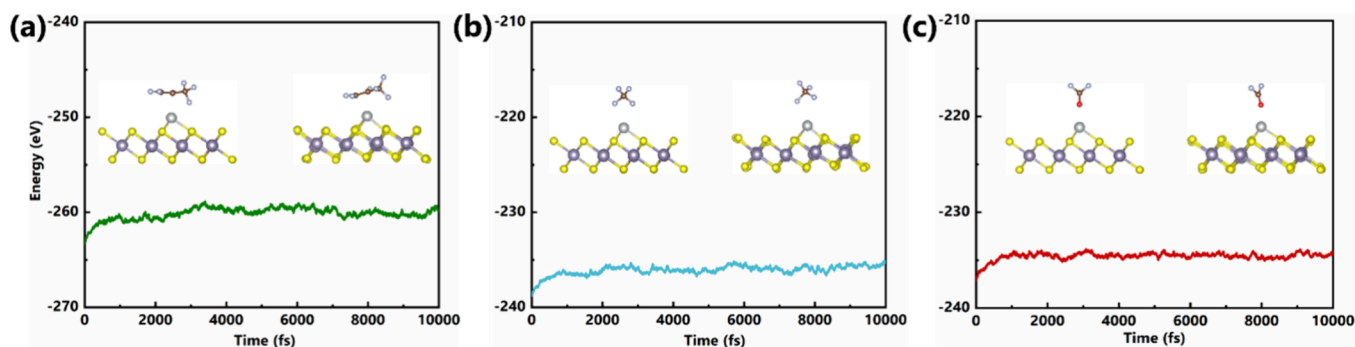


Figure 7. Adsorption stability of (a) C_3F_6 , (b) CF_4 , and (c) COF_2 molecules on the surface of $Ag-SnS_2$.

In stark contrast, interaction between COF_2 molecule and Ag atoms led to a reduced atomic gap of 2.434 \AA , a marginal Q_t of $-5.000 \times 10^{-4} e$, and a nearly tripled E_{ads} of $-3.178 \times 10^{-1} eV$. Concurrently, the C–O bond length underwent a slight expansion from 1.182 to 1.196 \AA . These parameters signified the most minimal gas–solid interfacial distance and the most pronounced adsorption strength among the six gas adsorption systems evaluated in this study. The pronounced interaction between the reactive carbonyl moiety ($C=O$) in COF_2 and the Ag atoms predominantly contributed to this observation. The PDOS graph in Figure 6c suggests that prior to Ag doping, the 2p orbitals of F atoms in COF_2 and the 3p orbitals of S atoms on the SnS_2 surface demonstrate noticeable overlaps at energies of -6.652 , -3.453 , and $-2.151 eV$. Conversely, in the $Ag-SnS_2$ system, the 4d orbitals of Ag and the 2p orbitals of O atoms exhibit significant overlap across various energy levels, namely, at -10.12 , -8.001 , -7.162 , -6.141 , and $-5.147 eV$, denoting a heightened state of hybridization, albeit not reaching the hybridization magnitude observed in the $C_3F_6/Ag-SnS_2$ adsorption system.

Adsorption Stability of Gas Molecules on the Surface of $Ag-SnS_2$. The presented analysis demonstrated that the E_{ads} 's of the three gas molecules on SnS_2 surfaces, irrespective of doping status, were comparatively low and did not achieve the threshold of chemical adsorption ($|E_{ads}| > 0.6 eV$). This phenomenon raised concerns about the potential instability of gas molecule adsorption during practical sensing operations, potentially resulting in diminished or erratic sensing responses. To address this, this work carried out molecular dynamics simulations on the $Ag-SnS_2$ surfaces to evaluate the adsorption stability of these gas molecules. Based on the NVT ensemble, we employed the Andersen thermostat method to investigate the thermal stability across various adsorption scenarios. These simulations were conducted at a steady temperature of 300 K (equivalent to room temperature) using a time step of 1 fs and extending over a total period of 10^5 fs . Figure 7 illustrates the energy fluctuations and structural alterations experienced by the three gas molecules after undergoing molecular dynamics calculations. Notably, C_3F_6 and CF_4 displayed energy variations of approximately $2.000 eV$, whereas COF_2 exhibited a more stable energy profile, consistently around $-234.5 eV$. In terms of structural changes, postsimulation analyses revealed that the nearest distances between C_3F_6 and COF_2 to the substrate diminish to 2.571 and 2.373 \AA , respectively. In contrast, the distance between CF_4 and the substrate expanded to 2.920 \AA , suggesting a propensity for disassociation. Consequently, inferring from the kinetic behavior of these gas molecules under ambient conditions, it appeared that C_3F_6 and COF_2 were capable of achieving stable adsorption on the

$Ag-SnS_2$ surface, whereas CF_4 was likely to disengage in a brief duration, failing to establish a dependable adsorption. Furthermore, optimal recovery characteristics are crucial for preventing sensor degradation and prolonging sensor lifespan. The recovery efficiency of sensors is generally quantified using the recovery time τ , which was computed as follows:⁴³

$$\tau = F^{-1} e^{-E_a/k_B T} \quad (3)$$

where F is the apparent frequency factor and defined as $10^{12} s^{-1}$ in this work. k_B and T are the Boltzmann constant ($eV \cdot K^{-1}$) and operating temperature (K), respectively. E_a represents the desorption energy barrier of the corresponding gas molecule. Calculated using eq 3, the recovery times for C_3F_6 , CF_4 , and COF_2 gases at ambient temperature are determined to be 1.381×10^{-16} , 7.172×10^{-15} , and $4.600 \times 10^{-18} s$, respectively, suggesting a swift desorption process for each gas from the $Ag-SnS_2$ surface.

Band Structure Analysis. To further analyze the impact of gas molecule adsorption on the conductivity of sensing materials, this study additionally computed the band structure of SnS_2 and $Ag-SnS_2$ before and after gas molecule adsorption. As evidenced in Figure 8, adsorption of all three gas molecules

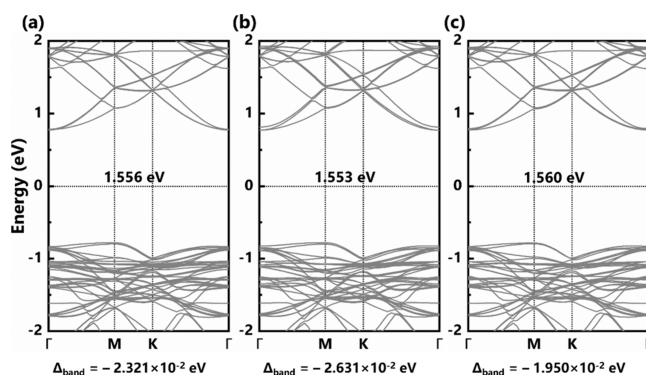


Figure 8. Band structures of pristine SnS_2 with (a) C_3F_6 , (b) CF_4 , and (c) COF_2 molecules adsorbed.

led to a reduction in the band gap of SnS_2 . This suggests that the energy barrier for electron excitation from the valence band to the conduction band will be lowered, resulting in a decrease in the resistance when these gases are detected in sensing experiments. Notably, the band gap change was most significant for CF_4 at $-2.631 \times 10^{-2} eV$ followed by C_3F_6 and COF_2 at $-2.321 \times 10^{-2} eV$ and $-1.950 \times 10^{-2} eV$, respectively. However, it is important to note that CF_4 exhibited considerably weaker adsorption stability than C_3F_6

and COF₂; thus, its actual contribution to changes in material conductivity might be lower than the theoretical value. In the Ag-SnS₂ adsorption systems (Figure 9), the band gap increased

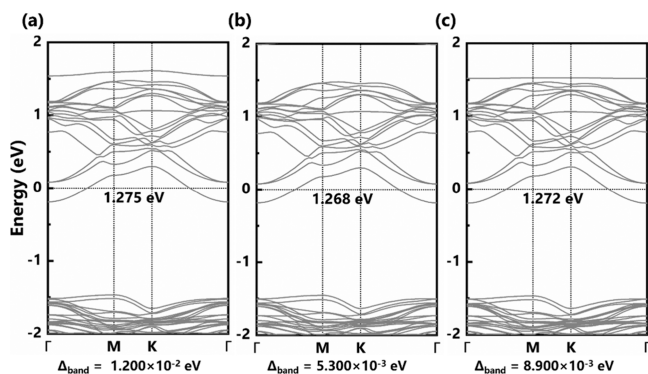


Figure 9. Band structures of Ag-SnS₂ with (a) C₃F₆, (b) CF₄, and (c) COF₂ molecules adsorbed.

for all three gases postadsorption, indicating a decrease in conductivity. In this scenario, C₃F₆ has the most significant impact on the band gap of Ag-SnS₂, increasing it by 1.200×10^{-2} eV, whereas the increases for COF₂ and CF₄ are smaller at 8.900×10^{-3} and 5.300×10^{-3} eV, respectively. Therefore, in the adsorption calculations of SnS₂ before and after Ag doping, CF₄ presented certain issues in adsorption stability, COF₂ contributed less to conductivity changes, and C₃F₆ can stably adsorb and alter the electronic structure of the sensing material. Theoretically, C₃F₆ exhibited the highest and most stable response among the three gases, suggesting a high potential for Ag-SnS₂ as a sensing material for C₃F₆ detection.

CONCLUSIONS

In this study, the performance and related mechanisms of intrinsic and Ag-doped SnS₂ adsorbing C₃F₆, CF₄, and COF₂ were comprehensively analyzed through DFT calculations of geometric and electronic parameters. The main conclusions drawn can be summarized as follows:

- i. Doping SnS₂ with Ag atoms significantly alters its electronic structure and enhances its conductivity.
- ii. Compared to intrinsic SnS₂, the introduction of Ag atoms improves the interaction strength at the gas–solid interface, leading to more stable adsorption of target gas molecules.
- iii. The adsorption of all three gas molecules on the modified SnS₂ surface does not reach the level of chemical adsorption, with the adsorption strength ranking as COF₂ > C₃F₆ > CF₄. Molecular dynamics simulations indicate that COF₂ and C₃F₆ can stably adsorb on the Ag-SnS₂ surface, whereas CF₄ tends to detach from the sensor surface;
- iv. Combining band gap analysis and recovery capability, it is found that CF₄ and COF₂ are weaker than C₃F₆ in terms of adsorption stability and band gap change contributions, respectively. Therefore, Ag-SnS₂ demonstrates potential for application as a C₃F₆ sensor.

ASSOCIATED CONTENT

Data Availability Statement

The data underlying this study are available in the published article.

AUTHOR INFORMATION

Corresponding Author

Peng Wu – School of Electrical Engineering and Automation, Wuhan University, Wuhan 430072, China; orcid.org/0000-0001-8578-5051; Email: wupeng@whu.edu.cn

Authors

Xiangyu Tan – Power Science Research Institute of Yunnan Power Grid Co., Ltd., Kunming 650214, China
 Zhimin Na – Qujing Power Supply Bureau of Yunnan Power Grid Co., Ltd., Qujing 655099, China
 Ran Zhuo – Electric Power Research Institute, China Southern Power Grid, Guangzhou 510623, China
 Fangrong Zhou – Power Science Research Institute of Yunnan Power Grid Co., Ltd., Kunming 650214, China
 Dibo Wang – Electric Power Research Institute, China Southern Power Grid, Guangzhou 510623, China
 Longchang Zhu – Power Science Research Institute of Yunnan Power Grid Co., Ltd., Kunming 650214, China

Complete contact information is available at:

<https://pubs.acs.org/10.1021/acsomega.4c00687>

Notes

The authors declare no competing financial interest.

ACKNOWLEDGMENTS

This work was supported by the science and technology project of China Southern Power Grid (grants YNKJXM20222118, YNKJXM20222131, and YNKJXM20222043).

REFERENCES

- (1) Zheng, C.; Zhang, C.; Zhang, K.; Zhang, J.; Jin, L.; Asiri, A. M.; Alamry, K. A.; He, L.; Chu, X. Growth of ZnFe₂O₄ nanosheets on reduced graphene oxide with enhanced ethanol sensing properties. *Sens. Actuators, B* **2021**, *330*, No. 129280.
- (2) Hu, J.; Chen, M.; Rong, Q.; Zhang, Y.; Wang, H.; Zhang, D.; Zhao, X.; Zhou, S.; Zi, B.; Zhao, J.; Zhang, J.; Zhu, Z.; Liu, Q. Formaldehyde sensing performance of reduced graphene oxide-wrapped hollow SnO₂ nanospheres composites. *Sens. Actuators, B* **2020**, *307*, No. 127584.
- (3) Chen, L.; Zhang, B.; Yang, T.; Deng, Y.; Li, X.; Murphy, A. B. Thermal decomposition characteristics and kinetic analysis of C₄F₇N/CO₂ gas mixture. *J. Phys. D: Appl. Phys.* **2020**, *53* (5), No. 055502.
- (4) Fang, X.; Hu, X.; Janssens-Maenhout, G.; Wu, J.; Han, J.; Su, S.; Zhang, J.; Hu, J. Sulfur hexafluoride (SF₆) emission estimates for China: an inventory for 1990–2010 and a projection to 2020. *Environ. Sci. Technol.* **2013**, *47* (8), 3848–3855.
- (5) Rabie, M.; Franck, C. M. Assessment of Eco-friendly Gases for Electrical Insulation to Replace the Most Potent Industrial Greenhouse Gas SF₆. *Environ. Sci. Technol.* **2018**, *52* (2), 369–380.
- (6) Zhang, X.; Cui, Z.; Li, Y.; Xiao, H.; Li, Y.; Tang, J.; Xiao, S. Abatement of SF₆ in the presence of NH₃ by dielectric barrier discharge plasma. *J. Hazard Mater.* **2018**, *360*, 341–348.
- (7) Huang, L.; Shen, Y.; Dong, W.; Zhang, R.; Zhang, J.; Hou, H. A novel method to decompose two potent greenhouse gases: photo-reduction of SF₆ and SF₅CF₃ in the presence of propene. *J. Hazard Mater.* **2008**, *151* (2–3), 323–330.
- (8) Wu, P.; Li, Y.; Xiao, S.; Chen, D.; Chen, J.; Tang, J.; Zhang, X. Room-Temperature Detection of Perfluoroisobutyronitrile with SnO₂/Ti₃C₂T_x Gas Sensors. *ACS Appl. Mater. Interfaces* **2022**, *14* (42), 48200–48211.
- (9) Zhang, B.; Li, C.; Xiong, J.; Zhang, Z.; Li, X.; Deng, Y. Decomposition characteristics of C₄F₇N/CO₂ mixture under AC discharge breakdown. *AIP Adv.* **2019**, *9* (11), 115212.

- (10) Guo, H.; Zheng, K.; Cui, H.; Zhang, F.; Yu, J.; Tao, L.-Q.; Li, X.; Chen, X. High sensitivity gas sensor to detect SF₆ decomposition components based on monolayer antimonide phosphorus. *Chem. Phys. Lett.* **2020**, 756, No. 137868.
- (11) Xiao, S.; Gao, B.; Pang, X.; Zhang, X.; Li, Y.; Tian, S.; Tang, J.; Luo, Y. The sensitivity of C₄F₇N to electric field and its influence to environment-friendly insulating gas mixture C₄F₇N/CO₂. *J. Phys. D* **2021**, 54 (5), No. 055501.
- (12) Gui, Y.; Zhang, X.; Lv, P.; Wang, S.; Tang, C.; Zhou, Q. Ni-CNT Chemical Sensor for SF₆ Decomposition Components Detection: A Combined Experimental and Theoretical Study. *Sensors* **2018**, 18 (10), 3493.
- (13) Li, Y.; Zhang, X.; Ye, F.; Chen, D.; Tian, S.; Cui, Z. Influence regularity of O₂ on dielectric and decomposition properties of C₄F₇N-CO₂-O₂ gas mixture for medium-voltage equipment. *High Voltage* **2020**, 5 (3), 256–263.
- (14) Ye, F.; Zhang, X.; Li, Y.; Yao, Y.; Xiao, S.; Zhang, X.; Xie, C.; Shao, X.; Sun, X. Effect of O₂ on AC Partial Discharge and Decomposition Behavior of C₄F₇N/CO₂/O₂ Gas Mixture. *IEEE Transactions on Dielectrics and Electrical Insulation* **2021**, 28 (4), 1440–1448.
- (15) Li, Y.; Zhang, X.; Li, Y.; Chen, D.; Cui, Z.; Liu, W.; Tang, J. Interaction Mechanism between the C₄F₇N-CO₂ Gas Mixture and the EPDM Seal Ring. *ACS Omega* **2020**, 5 (11), 5911–5920.
- (16) Ye, F.; Zhang, X.; Xie, C.; Sun, X.; Wu, P.; Xiao, S.; Tang, J.; Li, Y. Effect of Oxygen and Temperature on Thermal Decomposition Characteristics of C₄F₇N/CO₂/O₂ Gas Mixture for MV Equipment. *IEEE Access* **2020**, 8, 221004–221012.
- (17) Kumbhakar, P.; Chowde Gowda, C.; Mahapatra, P. L.; Mukherjee, M.; Malviya, K. D.; Chaker, M.; Chandra, A.; Lahiri, B.; Ajayan, P. M.; Jariwala, D.; Singh, A.; Tiwary, C. S. Emerging 2D metal oxides and their applications. *Mater. Today* **2021**, 45, 142–168.
- (18) Liu, J.; Zhang, L.; Fan, J.; Yu, J. Semiconductor Gas Sensor for Triethylamine Detection. *Small* **2021**, 18 (11), 2104984.
- (19) Ma, Y. T.; Ma, S. Y.; Tang, J.; Wu, Z. G.; Shi, J.; Zhao, Y.; Pei, S. T. One-pot hydrothermal method synthesised SnS/rGO nanocomposite under PVDF bonding for high-performance acetone gas sensor. *Materials Science and Engineering: B* **2021**, 263, No. 114861.
- (20) Qiu, P.; Qin, Y.; Wang, X. S-Vacancies and Ag Nanoparticles in SnS₂ Nanoflakes for Ethanol Sensing: A Combined Experimental and Theoretical Investigation. *ACS Applied Nano Materials* **2022**, 5 (8), 10839–10847.
- (21) Guo, X.; Zhang, F.; Zhang, Y.; Hu, J. Review on the advancement of SnS₂ in photocatalysis. *Journal of Materials Chemistry A* **2023**, 11 (14), 7331–7343.
- (22) Mishra, R. K.; Choi, H. J.; Ryu, J. W.; Choi, G. J.; Kumar, V.; Kumar, P.; Singh, J.; Kumar, S.; Gwag, J. S. Recent Progress in Gas Sensing based on 2D SnS₂ and its Heterostructures Platforms: A Review. *Sensors and Actuators A: Physical* **2024**, 365, No. 114860.
- (23) Liu, D.; Tang, Z.; Zhang, Z. Visible light assisted room-temperature NO₂ gas sensor based on hollow SnO₂@SnS₂ nanostructures. *Sens. Actuators, B* **2020**, 324, No. 128754.
- (24) Eom, T. H.; Cho, S. H.; Suh, J. M.; Kim, T.; Lee, T. H.; Jun, S. E.; Yang, J. W.; Lee, J.; Hong, S.-H.; Jang, H. W. Substantially improved room temperature NO₂ sensing in 2-dimensional SnS₂ nanoflowers enabled by visible light illumination. *Journal of Materials Chemistry A* **2021**, 9 (18), 11168–11178.
- (25) Giberti, A.; Gaiardo, A.; Fabbri, B.; Gherardi, S.; Guidi, V.; Malagù, C.; Bellutti, P.; Zonta, G.; Casotti, D.; Cruciani, G. Tin(IV) sulfide nanorods as a new gas sensing material. *Sens. Actuators, B* **2016**, 223, 827–833.
- (26) Huang, Y.; Jiao, W.; Chu, Z.; Wang, S.; Chen, L.; Nie, X.; Wang, R.; He, X. High Sensitivity, Humidity-Independent, Flexible NO₂ and NH₃ Gas Sensors Based on SnS₂ Hybrid Functional Graphene Ink. *ACS Appl. Mater. Interfaces* **2020**, 12 (1), 997–1004.
- (27) Qin, Z.; Xu, K.; Yue, H.; Wang, H.; Zhang, J.; Ouyang, C.; Xie, C.; Zeng, D. Enhanced room-temperature NH₃ gas sensing by 2D SnS₂ with sulfur vacancies synthesized by chemical exfoliation. *Sens. Actuators, B* **2018**, 262, 771–779.
- (28) Zhu, Q.; Gu, D.; Liu, Z.; Huang, B.; Li, X. Au-modified 3D SnS₂ nano-flowers for low-temperature NO₂ sensors. *Sens. Actuators, B* **2021**, 349, No. 130775.
- (29) Cui, X.; Xu, W.; Xie, Z.; Wang, Y. High-performance dye-sensitized solar cells based on Ag-doped SnS₂ counter electrodes. *J. Mater. Chem. A* **2016**, 4 (5), 1908–1914.
- (30) Yang, H.; Du, Z.; Yang, Y.; Wu, Q.; Ma, C.; Su, H.; Wang, X.; Zeng, D. Ce-Ag Active Bimetallic Pairs in Two-Dimensional SnS₂ for Enhancing NO₂ Sensing. *ACS Sens* **2024**, 9 (1), 283–291.
- (31) Yang, J.; Sun, L.; Hui, S.; Zhang, P.; Li, J.; Wang, D.; Wang, X.; Jiang, S. Ag functionalized SnS₂ with enhanced photothermal activity for safe and efficient wound disinfection. *Biomater Sci.* **2021**, 9 (13), 4728–4736.
- (32) Kresse, G.; Furthmüller, J. Efficiency of ab-initio total energy calculations for metals and semiconductors using a plane-wave basis set. *Comput. Mater. Sci.* **1996**, 6 (1), 15–50.
- (33) Kresse, G.; Furthmüller, J. Efficient iterative schemes for ab initio total-energy calculations using a plane-wave basis set. *Phys. Rev. B* **1996**, 54 (16), 11169–11186.
- (34) Perdew, J. P.; Burke, K.; Ernzerhof, M. Generalized Gradient Approximation Made Simple. *Phys. Rev. Lett.* **1996**, 77 (18), 3865–3868.
- (35) Grimme, S. Semiempirical GGA-type density functional constructed with a long-range dispersion correction. *J. Comput. Chem.* **2006**, 27 (15), 1787–1799.
- (36) Chen, G.-X.; Chen, X.-N.; Wang, D.-D.; An, G.; Zhang, J.-M. Sensing properties of NO₂ gas sensor based on nonmetal doped α -AsP monolayer: A first-principles study. *Materials Science in Semiconductor Processing* **2022**, 139 (1), No. 106319.
- (37) Pan, W.; Qi, N.; Zhao, B.; Chang, S.; Ye, S.; Chen, Z. Gas sensing properties of buckled bismuthene predicted by first-principles calculations. *Phys. Chem. Chem. Phys.* **2019**, 21 (21), 11455–11463.
- (38) Peng, X.; Liu, D.; Zhao, F.; Tang, C. Gas sensing properties of Mg-doped graphene for H₂S, SO₂, SOF₂, and SO₂F₂ based on DFT. *Int. J. Quantum Chem.* **2022**, 122 (22), No. e26989.
- (39) Guo, L.-Y.; Xia, S.-Y.; Sun, H.; Li, C.-H.; Long, Y.; Zhu, C.; Gui, Y.; Huang, Z.; Li, J. A DFT Study of the Ag-Doped h-BN Monolayer for Harmful Gases (NO₂, SO₂F₂, and NO). *Surfaces and Interfaces* **2022**, 32, No. 102113.
- (40) Bacaksiz, C.; Cahangirov, S.; Rubio, A.; Senger, R. T.; Peeters, F. M.; Sahin, H. Bilayer SnS₂: Tunable stacking sequence by charging and loading pressure. *Phys. Rev. B* **2016**, 93 (12), No. 125403.
- (41) Xu, L.; Zhu, H.; Gui, Y.; Long, Y.; Wang, Q.; Yang, P. First-Principles Calculations of Gas-Sensing Properties of Pd Clusters Decorated AlNNTs to Dissolved Gases in Transformer Oil. *IEEE Access* **2020**, 8 (1), 162692–162700.
- (42) Zhuang, H. L.; Hennig, R. G. Theoretical perspective of photocatalytic properties of single-layer SnS₂. *Phys. Rev. B* **2013**, 88 (11), No. 115314.
- (43) Peng, S.; Cho, K.; Qi, P.; Dai, H. Ab initio study of CNT NO₂ gas sensor. *Chem. Phys. Lett.* **2004**, 387 (4–6), 271–276.